ORIGINAL ARTICLE

A new radiomics approach combining the tumor and peri-tumor regions to predict lymph node metastasis and prognosis in gastric cancer

Yutao Yang[1], Hao Chen[2], Min Ji[3], Jianzhang Wu[2], Xiaoshan Chen[1], Fenglin Liu[2,4]* and Shengxiang Rao [ID] [5]*

[1]Department of Radiology, Zhongshan Hospital, Fudan University, Shanghai, P. R. China, [2]Department of General Surgery, Zhongshan Hospital, Fudan University, Shanghai, P. R. China, [3]Research Collaboration, Shanghai United Imaging Healthcare Co., Ltd., Shanghai, P. R. China, [4]Department of Cancer Center, Zhongshan Hospital, Fudan University, Shanghai, P. R. China; [5]Shanghai Institute of Medical Imaging, Shanghai, P. R. China

*Corresponding authors. Shengxiang Rao, Shanghai Institute of Medical Imaging, Shanghai 200032, P. R. China. Tel: +86-13764181846; Email: raoxray@163.com; Fenglin Liu, Department of General Surgery, Zhongshan Hospital, Fudan University, 180 Fenglin Road, Shanghai 200032, P. R. China. Tel: +86-13918765733; Email: liu.fenglin@zs-hospital.sh.cn

Abstract

Objective The development of non-invasive methods for evaluating lymph node metastasis (LNM) preoperatively in gastric cancer (GC) is necessary. In this study, we developed a new radiomics model combining features from the tumor and peri-tumor regions for predicting LNM and prognoses.

Methods This was a retrospective observational study. In this study, two cohorts of patients with GC treated in Zhongshan Hospital Fudan University (Shanghai, China) were included. In total, 193 patients were assigned to the internal training/validation cohort; another 98 patients were assigned to the independent testing cohort. The radiomics features were extracted from venous phase computerized tomography (CT) images. The radiomics model was constructed and the output was defined as the radiomics score (RS). The performance of the RS and CT-defined N status (ctN) for predicting LNM was compared using the area under the curve (AUC). The 5-year overall survival and progression-free survival were compared between different subgroups using Kaplan–Meier curves.

Results In both cohorts, the RS was significantly higher in the LNM-positive group than that in the LNM-negative group (all $P < 0.001$). The radiomics model combining features from the tumor and peri-tumor regions achieved the highest AUC in predicting LNM (AUC, 0.779 and 0.724, respectively), which performed better than the radiomics model based only on the tumor region and ctN (AUC, 0.717, 0.622 and 0.710, 0.603, respectively). The differences in 5-year overall survival and progression-free survival between high-risk and low-risk groups were significant (both $P < 0.001$).

Conclusions The radiomics model combining features from the tumor and peri-tumor regions could effectively predict the LNM in GC. Risk stratification based on the RS was capable of distinguishing patients with poor prognoses.

Key words: radiomics; lymph node metastasis; prognosis; gastric cancer

Introduction

Gastric cancer (GC) is the second leading cause of cancer-related death [1]. Lymph node metastasis (LNM) is important for cancer staging, which affects the selection of therapeutic methods and the evaluation of prognosis. In clinical practice, the status of the lymph node in GC is confirmed only by pathological examinations after surgery. A non-invasive tool that might enable us to detect LNM before surgery would be beneficial as it might allow further treatment optimization.

According to national guidelines (including NCCN [National Comprehensive Cancer Network], CSCO [Chinese Society of Clinical Oncology] guidelines *et al*.), endoscopic ultrasound (EUS) and computerized tomography (CT) scanning are recommended for determining the category of the nodes in GC. However, EUS can only be used to detect enlarged lymph nodes in the gastric-neighboring region [2, 3]. The accuracy of diagnosing LNM of GC by analysing CT images ranges from 61% to 64% [4, 5]. To our knowledge, a reliable method for preoperative evaluation of lymph nodes has not been established to date.

Radiomics has become a popular field of research in recent years. It is conducted by selecting valuable features among many quantitative features extracted from medical images and constructing the corresponding mathematical model to provide support for clinical decision-making. In many previous studies, radiomics models exhibited excellent performance in identifying LNM. In a study by Feng *et al.* [6], the radiomics model showed a relatively good discriminating ability in the training cohort with area under the curve (AUC) of 0.824, and AUC of 0.764 in the test cohort. A large multicenter study reported good discrimination of the number of metastatic lymph nodes using a deep learning-based radiomic nomogram, which reached C-indexes of 0.821 in the primary cohort and 0.797–0.822 in different validation cohorts [7]. Most of the radiomics-related studies about GC were performed on the tumor lesion, which reflects the biologic behavior of the tumor. On the other hand, the radiological information of surrounding tissues of GC such as extramural venous invasion etc. is associated with the invasiveness of the tumor, which might indicate the presence of LNM and poor prognosis [8]. Thus, we hope to establish a radiomics model based on the CT imaging characteristics from both the tumor lesion and the peri-tumor region to predict the occurrence of LNM. On this basis, we further explore whether the model can indirectly reflect patients' long-term survival and progression-free survival outcomes, which might help when performing risk stratification and implementing individualized treatment.

Methods

Study population

This was a retrospective observational study. In this study, data on 436 cases of GC patients were retrospectively collected. These patients had undergone preoperative contrast-enhanced abdominal CT scanning, radical gastrectomy, and extended lymph node dissection in Zhongshan Hospital, Fudan University (Shanghai, China) between January 2010 and April 2012. After further screening, 193 patients were finally enrolled in the internal training/validation cohort. Another 214 cases of GC from January 2019 to October 2019 in our institute who received preoperative abdominal CT scanning and had been confirmed by histopathology were collected and at last 98 cases

were enrolled as the independent testing cohort. The exclusion criteria were as follows: (i) a history of surgery or other primary cancer; (ii) a history of neoadjuvant chemoradiotherapy; (iii) patients who received chemotherapy or radiation therapy instead of surgery; (iv) post-operative pathological diagnosis such as gastrointestinal stromal tumor (GIST), neuroendocrine carcinoma, or intraepithelial neoplasia; (v) poorly dilated gastric cavity on CT images; (vi) difficulty in delineating the tumor lesion on CT images; (vii) the time interval between CT scanning and surgery beyond 2 weeks. The flow diagram of the patient inclusion and exclusion process is shown in Figure 1. This study was approved by the institutional review board of Zhongshan Hospital, Fudan University with a waiver of informed consent (approval number: B2020-081R).

Follow-up

All 193 patients in the internal training/validation cohort were followed up after surgery every 3 months within 2 years, every 6 months between 2 and 5 years, and every year after 5 years. The death of a patient or loss to follow-up was considered to be the end point of follow-up. All 98 patients in the independent testing cohort were followed up after surgery until October 2020. Any local recurrence or distant metastases observed by medical imaging, endoscopy, or laboratory examination, and death due to GC were defined as disease progression. The time interval between the first day after surgery and the last day of follow-up was recorded. The progression-free survival was defined as the time interval between surgery and the disease-progression status, or the most recent follow-up date for patients without any progression.

Acquisition of CT images

CT scanning of the 193 patients in the internal training/validation cohort was performed using the following machines: 16-slice multi-detector spiral CT (Somatom Sensation 16, Siemens Healthcare, Germany), 128-slice multi-detector spiral CT (Somatom Definition AS, Siemens Healthcare, Germany), and 64-slice multi-detector spiral CT (Lightspeed VCT, GE Healthcare, Milwaukee, Wisconsin, USA). CT scanning of the 98 patients in the independent testing cohort was performed on a 128-slice multi-detector spiral CT machine (Somatom Definition AS, Siemens Healthcare, Germany). All patients fasted for at least 8 hours before CT scanning and consumed 800–1,000 mL of water 20 minutes before the examination to fully distend the stomach. The scanning area ranged from the top of the diaphragm to the level of the symphysis pubis with patients in the supine position. About 100 mL of nonionic contrast agent (300 mg I/mL; Ultravist, Bayer Schering Pharma, Berlin, Germany) was injected at a rate of 3 mL/s from the elbow vein using a high-pressure injector. Then, the patients underwent CT scanning 30–35 and 80 s relatively after the injection to obtain arterial and venous phase CT images using auto-trigger technology. The CT scan parameters were as follows: detector collimation of 16×0.75 mm (Somatom Sensation 16, Siemens Healthcare), 32×1.2 mm (Somatom Definition AS, Siemens Healthcare), and 64×0.625 mm (Lightspeed VCT, GE Healthcare); tube current of 160 mAs (Somatom Sensation 16 and Somatom Definition AS, Siemens Healthcare) and 100–300 mAs automatic tube current modulation (Lightspeed VCT, GE Healthcare); tube voltage of 120 kVp; frame rotation time of 0.5 s; imaging matrix size of 512×512; slice thickness of 5 mm; slice spacing of 5 mm. All CT images were transmitted to the Picture Archiving and
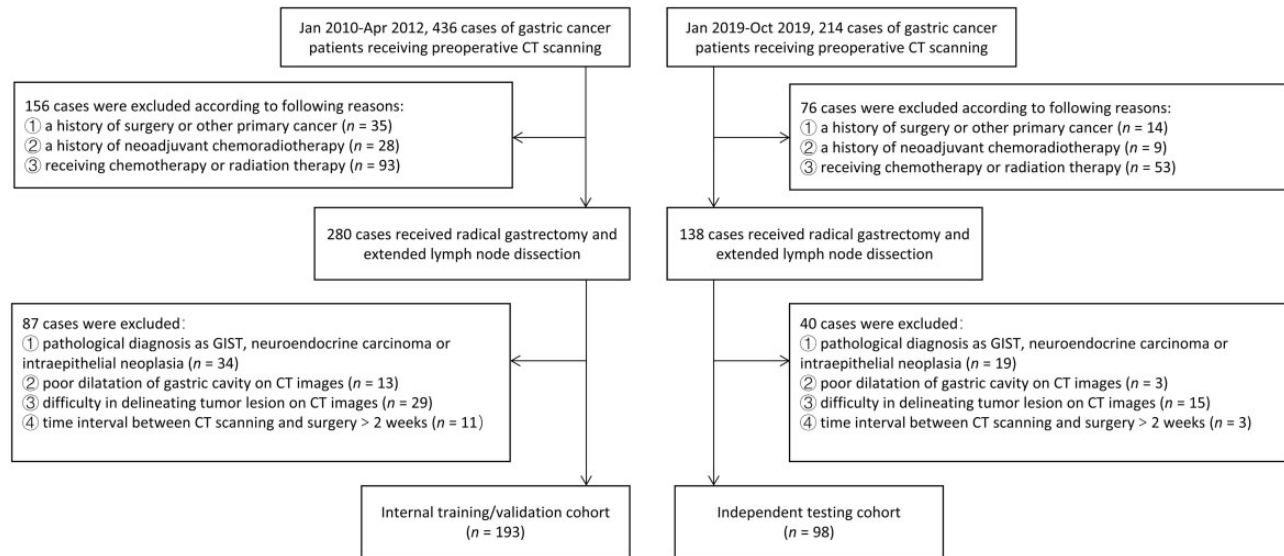
Figure 1. A flow diagram of the patient inclusion and exclusion process. CT, computerized tomography; GIST, gastrointestinal stromal tumor.

Communication System (Centricity, GE Healthcare Systems, Milwaukee, Wisconsin, USA) in our department.

CT image analysis

Two readers independently evaluated the morphological CT features. They were only informed that the patients were of GC and they were unaware of the post-operative histopathological reports. According to the eighth edition of the AJCC (American Joint Committee on Cancer) cancer-staging manual, the celiac lymph node observed on CT images with maximum short diameter of >10 mm was considered to have metastasized, which was defined as ctN-positive status [9]. Two readers evaluated the ctN status of each patient respectively. In case of a disagreement between the doctors, a final decision was made after discussion. The thickest diameter of the tumor was measured based on axial venous phase CT images by two readers respectively. The parameter was defined as the longest distance between the inner and outer walls of the tumor lesion.

Image segmentation

The segmentation of the tumor area was performed slice by slice using the 5-mm-thickness venous phase CT images by one reader and the operation was confirmed by another reader. In case of a disagreement regarding the process of segmentation, the two readers reached a consensus after consultation. During the process of image segmentation, two readers were told the location of the tumor lesion, although they were unaware of the specific clinical and histopathological information. The volume of interest (VOI) of GC was determined using open-source software LIFEx (version 5.10). The VOI of the tumor was determined carefully, avoiding water or gas in the gastric cavity, as well as the intestinal tract surrounding the stomach, adjacent organs and tissues, and large blood vessels. The topmost and bottommost images of the tumor were excluded to minimize potential bias due to partial volume effects. After delineating the tumor region, a 5-mm area around the tumor region was semi-automatically sketched by using LIFEx software. The intestinal tract, adjacent organs, and large vessels within the 5-mm area

were removed by using manual correction. The VOI of the tumor region was denoted as C1 and the VOI of the 5-mm peritumor region was denoted as C2. The process of delineating the VOI is shown in Figure 2.

Extraction of the radiomics features

The radiomics features were extracted from the delineated region using functions provided by LIFEx 5.10 software. The CT images were resampled to $1 \times 1 \times 1$ mm voxels. The Hounsfield units in all images were resampled into 400 discrete values (called bin) with absolute discreteness ranging from −1,000 to 3,000 [10]. We extracted 49 imaging features from both tumor region C1 and peri-tumor region C2. Of these, 17 were first-order features, which included 4 morphological features, 6 histogram features, and 7 traditional features; and 32 were second-order features, which included 7 gray-level co-occurrence matrix features (GLCM), 11 gray-level run-length matrix features (GLRLM), 3 neighboring gray-level dependence matrix features (NGLDM), and 11 gray-level zone-length matrix features (GLZLM).

Construction of the radiomics models

The least absolute shrinkage and selection operator regularization logistic regression analysis was performed to determine the most stable features for distinguishing the positive/negative LNM status. While constructing the model, the λ parameter was regulated and the regularization intensity was controlled. The penalty parameters were adjusted by a 10-fold cross-validation method to select stable and non-redundant features from the internal training/validation cohort. Finally, 16 features were selected out of 49 features from tumor region C1, and 28 features were selected out of the overall 98 features from tumor region C1 and the peripheral 5-mm region C2. The selected features were weighted in a linear combination based on their respective coefficients to create a radiomics model, and the corresponding radiomics score (RS) was calculated for each patient. The RS calculated from the model based on the tumor region was recorded as RS (C1), and the RS based on the
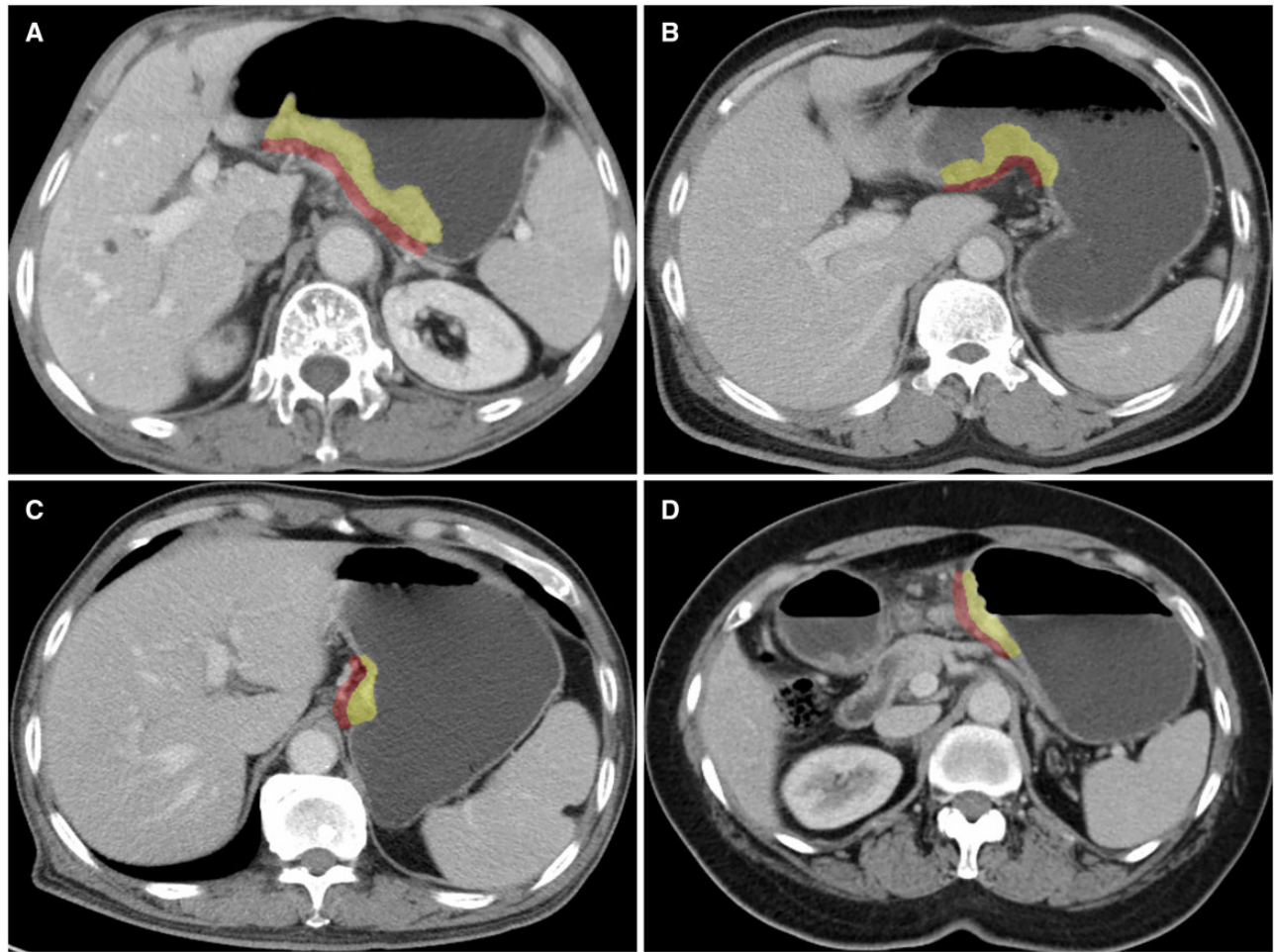
Figure 2. Examples of manually sketching the region of interest at a certain venous phase CT slice. The tumor lesion was delineated as the yellow region (C1) and the 5-mm peri-tumor tissue was delineated as the red region (C2). (A) A 77-year-old man with gastric body cancer in the internal training/validation cohort, stratified as a high-risk patient with a RS (C1+C2) value of 2.03. No lymph node metastasis was found by post-operative pathological examinations. The post-operative survival time was 12 months. (B) A 57-year-old man with gastric body cancer in the internal training/validation cohort, stratified into the low-risk group with a RS (C1+C2) value of 0.05. Pathological examinations confirmed the occurrence of lymph node metastasis. The survival time was >5 years. (C) A 73-year-old man with gastric cardia cancer in the independent testing cohort stratified as a low-risk patient with a RS (C1+C2) value of 1.17. No lymph node metastasis was found by pathological examinations. No disease progression was found during the follow-up period. (D) A 63-year-old woman with gastric body cancer in the independent testing cohort, stratified into the high-risk group with an RS (C1+C2) value of 4.10. The CT images showed enlarged lymph nodes around the tumor. The pathological examinations showed the occurrence of lymph node metastasis. This patient developed disease progression a week after surgery. RS (C1), radiomics score (C1); RS (C1+C2), radiomics score (C1+C2).

tumor region combined with the 5-mm peripheral region was recorded as RS (C1+C2).

Statistical analysis

The inter-reader correlation coefficient (ICC) was analysed for measuring the thickest diameter of the tumor by two readers. The clinical and CT characteristics of LNM-positive and LNM-negative patients in the two cohorts were compared. Multivariate logistic regression analysis was performed on CT features in both cohorts, before which a multicollinearity test was performed on all variables. The receiver operator characteristic (ROC) curve was used to analyse the diagnostic efficacy of the ctN and radiomics scores RS1 and RS2 for LNM. The X-tile software (Yale School of Medicine, New Haven, USA) was used for determining the best cut-off value of RS (C1+C2) for predicting 5-year overall survival and progression-free survival. Kaplan–Meier curves were plotted to compare the survival outcomes of the high-risk and low-risk groups. Statistical analyses

were performed using the SPSS 25.0 software (IBM Corp, Armonk, USA) and MedCalc version 16.8.4 (MedCalc Software Ltd, Ostend, Belgium). A two-tailed P-value of <0.05 indicated the significance of statistical results.

Results

Clinical information and CT characteristics

A total of 132 men and 61 women were enrolled in the internal training/validation cohort, with a mean age of 63.48 ± 10.60 years (range, 36–92 years). The independent testing cohort included 67 men and 31 women, with a mean age of 63.87 ± 9.55 years (range, 28–84 years). No distant metastasis was observed in the preoperative CT scans and intraoperative exploration. The clinical information and CT characteristics were compared between LNM-positive and LNM-negative groups in both cohorts (Table 1). The patients in the LNM-positive and LNM-negative groups did not have significant differences in age

Table 1. Clinical and CT characteristics in internal training/validation cohort ($n = 193$) and independent testing cohort ($n = 98$)

Characteristic	Internal training/validation cohort			Independent testing cohort		
	LNM-positive ($n = 107$)	LNM-negative ($n = 86$)	P	LNM-positive ($n = 57$)	LNM-negative ($n = 41$)	P
Age, mean $\pm$ SD, year	63.08 $\pm$ 10.89	63.98 $\pm$ 10.28	0.606	64.19 $\pm$ 9.52	63.41 $\pm$ 9.70	0.552
Gender, n (%)			0.193			0.371
Male	69 (64.5)	63 (73.3)		41 (71.9)	26 (63.4)	
Female	38 (35.5)	23 (26.7)		16 (28.1)	15 (36.6)	
Location of tumor, n (%)			0.073			0.361
Cardia	18 (16.8)	13 (15.1)		14 (24.6)	10 (24.4)	
Body	37 (34.6)	18 (20.9)		18 (31.6)	8 (19.5)	
Antrum	52 (48.6)	55 (64.0)		25 (43.8)	23 (56.1)	
Thickest diameter, mean $\pm$ SD, mm	19.50 $\pm$ 6.54	17.84 $\pm$ 6.74	0.051	18.83 $\pm$ 6.00	14.70 $\pm$ 5.96	<0.001
ctN, n (%)			0.001			0.044
Positive	56 (52.3)	24 (27.9)		34 (59.6)	16 (39.0)	
Negative	51 (47.7)	62 (72.1)		23 (40.4)	25 (61.0)	
RS (C1), mean $\pm$ SD	0.39 $\pm$ 0.48	0.04 $\pm$ 0.45	<0.001	1.27 $\pm$ 0.85	0.76 $\pm$ 0.73	<0.001
RS (C1+C2), mean $\pm$ SD	0.62 $\pm$ 0.76	−0.19 $\pm$ 0.79	<0.001	2.77 $\pm$ 1.56	1.66 $\pm$ 1.41	<0.001

CT, computerized tomography; LNM, lymph node metastasis; SD, standard deviation; ctN, CT-defined N status; RS (C1), radiomics score (C1); RS (C1+C2), radiomics score (C1+C2).

($P = 0.606$ [internal training/validation cohort]; $P = 0.552$ [independent testing cohort]), gender ($P = 0.193$ [internal training/validation cohort]; $P = 0.371$ [independent testing cohort]), and tumor location ($P = 0.073$ [internal training/validation cohort]; $P = 0.361$ [independent testing cohort]).

The ICC value of the thickest diameter of the tumor measured by two readers was 0.814. Good consistency was achieved between the readers, considering that the ICC value was >0.75. In the training/validation cohort, the mean maximum tumor diameter in the LNM-positive group was 19.50 ± 6.54 mm, and that in the LNM-negative group was 17.84 ± 6.74 mm. The difference in the tumor diameter between two groups was not significant ($P = 0.051$). In the testing cohort, the differences in the mean maximum tumor diameter between the LNM-positive group (18.83 ± 6.00 mm) and the LNM-negative group (14.70 ± 5.96 mm) was significant ($P < 0.001$). In the training/validation cohort, the frequency of the ctN-positive status was significantly higher in the LNM-positive group than in the LNM-negative group (52.3% vs 27.9%, $P < 0.001$). In the testing group, the frequency of the ctN-positive status in the LNM-positive group was also significantly higher than that in the LNM-negative group (59.6% vs 39.0%, $P = 0.044$). The differences in the RS between the LNM-positive and LNM-negative groups were significant. In both cohorts, the RS values of the LNM-positive group were significantly higher than those of the LNM-negative group for the tumor region alone (RS [C1]) and the tumor area combined with the peri-tumor region (RS [C1+C2]) (all $P < 0.001$).

Efficiency for predicting LNM

The efficiency for predicting LNM based on the ctN status and RS (C1) and RS (C1+C2) was compared by performing the ROC analysis. The ROC curves are shown in Figure 3 and the results of the comparison are provided in Table 2. It was found that the AUCs of the RSs were higher in both cohorts. Additionally, the RS (C1+C2) value based on the tumor region and combined with peri-tumor tissue had the highest AUC, which was 0.779 (95% confidence interval [CI], 0.713–0.835) in the training/validation cohort and 0.724 (95% CI, 0.625–0.810) in the testing cohort. Compared to ctN, the AUC of the RS (C1+C2) value had

increased by 0.157 in the training/validation cohort and 0.121 in the testing cohort, with significant different P-values of <0.001 and <0.026, respectively. Compared with the RS (C1) value, the AUC of the RS (C1+C2) value had notably increased by 0.062 in the training/validation cohort ($P = 0.007$) and 0.014 in the testing cohort, whereas the difference between the two was not significant ($P = 0.660$).

Risk factors for LNM

The ctN status, thickest diameter of the tumor, and RS (C1+C2) value were included in the multivariate logistic regression analysis. The results are shown in Table 3. In the training/validation cohort, the RS (C1+C2) value was an independent risk factor for LNM in GC (odds ratio [OR], 4.502; 95% CI, 2.572–7.880; $P < 0.001$). However, none of these three factors was an independent risk factor in the testing cohort, but the RS (C1+C2) value showed a critical positive trend (OR, 1.435; 95% CI, 0.979–2.104, $P < 0.064$).

Capability for evaluating prognosis

The X-tile software was used to determine the best cut-off value of the RS (C1+C2) value for predicting 5-year survival of the patients in the training/validation cohort and the progression-free survival of the patients in the testing cohort. The patients were classified into low-risk and high-risk groups, with a cut-off value of 0.19 in the training/validation cohort and 4.08 in the testing cohort. Higher RSs indicated poorer prognoses in both cohorts. In the training/validation cohort, the mean overall survival time was 58.43 months (95% CI, 56.92–59.94) for the low-risk group and 40.26 months (95% CI, 36.34–44.19) for the high-risk group. In the testing cohort, the mean progression-free survival time was 13.51 months (95% CI, 12.48–14.54) for the low-risk group and 8.28 months (95% CI, 4.63–11.91) for the high-risk group. The Kaplan–Meier survival analysis was performed between different risk groups and the results are shown in Figure 4. For the training/validation cohort, the 5-year overall survival differed significantly between the high-risk and low-risk groups (log-rank test: $\chi^2 = 58.61$, $P < 0.001$). The
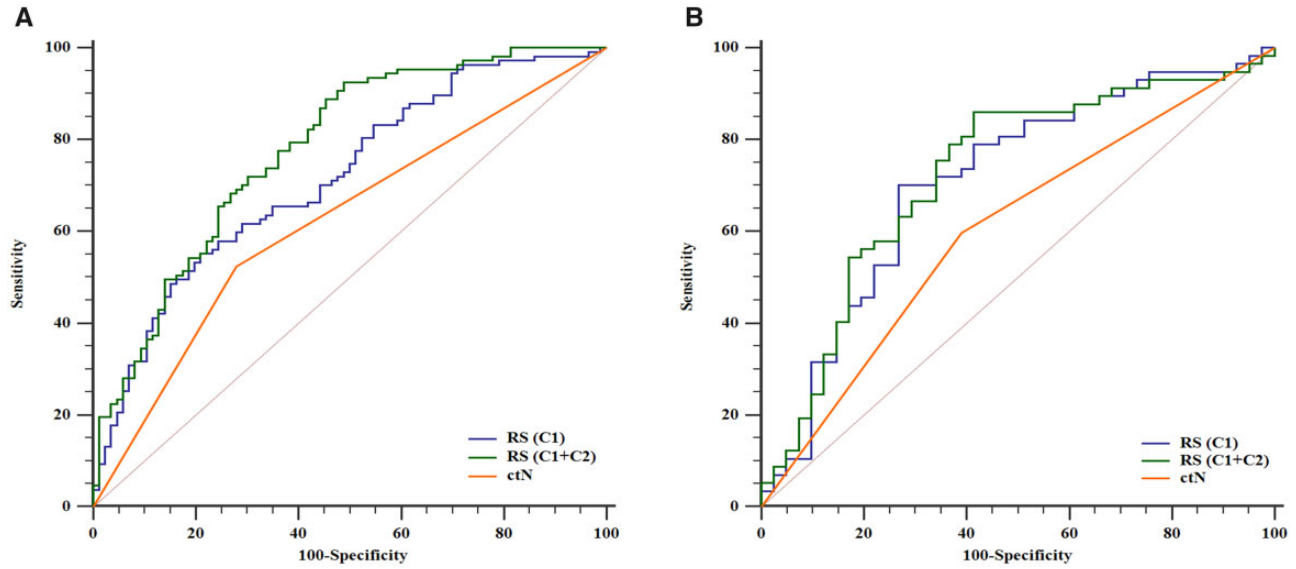
Figure 3. Comparisons among the ROC curves of RS (C1), RS (C1+C2), and ctN for predicting lymph node metastasis. (A) The ROC curves of three characteristics in the internal training/validation cohort. (B) The ROC curves of three characteristics in the independent testing cohort. ROC, receiver operator characteristic curve; RS (C1), radiomics score (C1); RS (C1+C2), radiomics score (C1+C2); ctN, CT-defined N status.

Table 2. Comparisons among AUCs of ctN, RS (C1), and RS (C1+C2) for predicting lymph node metastasis

Factor	Internal training/validation cohort			Independent testing cohort		
	AUC (95% CI)	△AUC	P	AUC (95% CI)	△AUC	P
ctN	0.622 (0.550–0.691)	–	–	0.603 (0.499–0.701)	–	–
RS (C1)	0.717 (0.648–0.779)	0.095	0.029	0.710 (0.610–0.797)	0.107	0.067
RS (C1+C2)	0.779 (0.713–0.835)	0.157	<0.001	0.724 (0.625–0.810)	0.121	0.026

AUC, area under the curve; ctN, CT-defined N status; RS (C1), radiomics score (C1); RS (C1+C2), radiomics score (C1+C2); CI, confidence interval. △AUC represents the difference between the AUC of other factors and ctN.

Table 3. Multivariate analysis of risk factors for lymph node metastasis

Factor	Internal training/validation cohort		Independent testing cohort	
	OR (95% CI)	P	OR (95% CI)	P
ctN	1.602 (0.798–3.217)	0.185	0.977 (0.360–2.652)	0.964
Thickest diameter of tumor	0.965 (0.913–1.020)	0.208	1.083 (0.982–1.194)	0.112
RS (C1+C2)	4.502 (2.572–7.880)	<0.001	1.435 (0.979–2.104)	0.064

OR, odds ratio; CI, confidence interval; RS (C1+C2), radiomics score (C1+C2).

progression-free survival also differed significantly between the high-risk and low-risk groups in the independent test cohort (log-rank test: $\chi^2 = 10.94$, $P < 0.001$).

Discussion

The radiological features of the surrounding tissues of a gastric tumor lesion can reflect certain biological behaviors of the tumor [8]. In this study, we established two different radiomics models: one was based on features from the tumor region alone and the other was based on the tumor region and 5-mm peritumor tissue, which contained 16 and 28 robust features, respectively. We found that the RS (C1+C2) value based on the second model showed good efficiency for predicting LNM, which was not only better than the ctN status based on the

node size (internal training/validation cohort, $P < 0.001$; independent testing cohort, $P = 0.026$), but also better than the RS (C1) value merely based on the tumor region (internal training/validation cohort, $P = 0.007$).

It is still challenging to estimate LNM by simply depending on morphological features. In our study, the AUC of the ctN status in diagnosing LNM was 0.622 in the training/validation cohort and 0.603 in the testing cohort, which indicated relatively poor efficiency. The ctN status was not reliable for the differential diagnosis, especially in patients with LNM, reaching a true positive rate of 52.3% and 59.6%, and an accuracy of 61.14% and 60.20%, in 107 cases of LNM-positive patients in the training/validation cohort and 57 cases of LNM-positive patients in the testing cohort, respectively. In a study by Wang *et al.*, the accuracy of ctN in evaluating LNM of GC is ~62% [11], which was
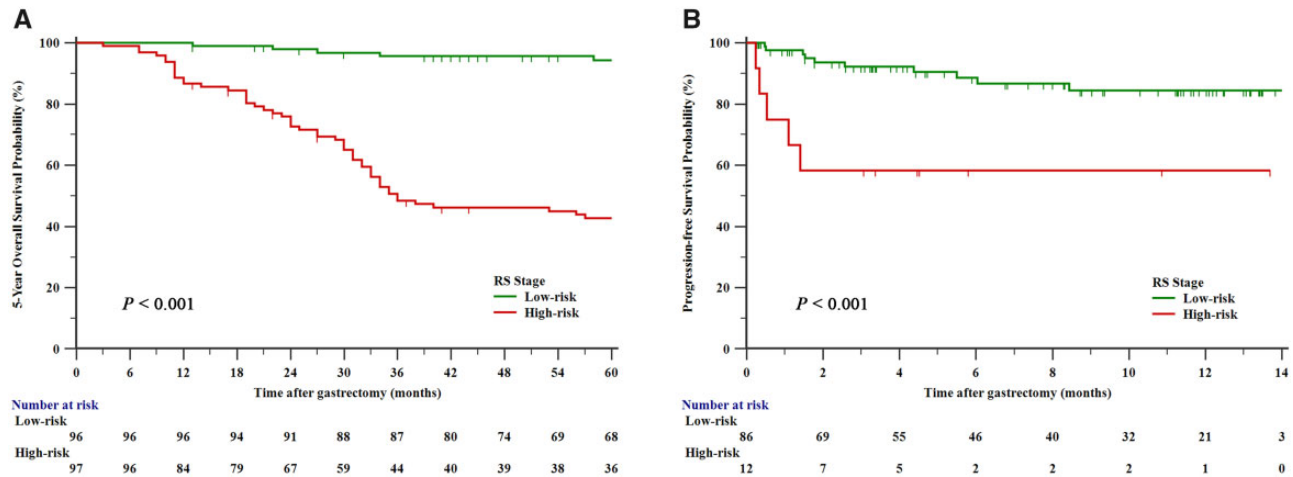
Figure 4. Kaplan–Meier curves for 5-year overall survival and progression-free survival in different risk groups stratified according to the radiomics score. (A) The 5-year overall survival in the internal training/validation cohort. (B) The progression-free survival of the patients in the independent testing cohort. RS, radiomics score.

similar to our results. These data showed that accurately identifying the true status of LNM based only on morphological features of lymph nodes is difficult, since small nodular metastases can occur in the lymph nodes, as well as non-specific hyperplasia and enlargement of the inflammatory nodes [12–14]. PET/CT can be performed to obtain information on metabolism, which might improve the detection of LNMs that are not prominent in conventional CT scans. However, the sensitivity is low (49%), as reported in another study [15].

The heterogeneity within a tumor suggests a high tendency for metastasis [16]. CT images contain quantities of high-dimensional features that cannot be assessed visually, but the information might reflect the biological behavior of the tumor. Radiomics can help to extract such information. Many studies have proven that a radiomics model can help to reflect the heterogeneity inside a tumor and evaluate the aggressiveness of the tumor in many clinical situations [17]. In our study, 28 radiomics features were included in the model based on the tumor region combined with the 5-mm peripheral region. Of the 15 features from the tumor region, 9 features (GLCM_Homogeneity, GLCM_Correlation, GLRLM_LRHGE, NGLDM_Coarseness, NGLDM_Busyness, GLZLM_SZE, GLZLM_LZLGE, GLZLM_GLNU, and GLZLM_ZP) described the pattern and spatial distribution of the voxel intensity of the region of interest. In contrast, 10 of the 13 features from the 5-mm peripheral region (GLCM_Homogeneity, GLCM_Correlation, GLRLM_GLNU, GLRLM_RLNU, NGLDM_Coarseness, NGLDM_Busyness, GLZLM_SZE, GLZLM_GLNU, GLZLM_ZLNU, and GLZLM_ZP) provided such information. These features reflected the interactions between adjacent pixels in the tumor region, with specific formulae to quantify the texture heterogeneity of the different aspects, which might partially indicate the biological heterogeneity within the tumor [18].

Concerning the ability to predict LNM, the RS (C1+C2) values in both cohorts reached the maximum AUC (0.779 and 0.724). Compared with many previous radiomics studies on GC, we further constructed a model combining the features from both the tumor region and the surrounding 5-mm tissue. In a radiomics study about distinguishing adenocarcinomas and granulomas on lung CT, the most predictive features were found to be within the peripheral 5-mm distance from the nodule [19]. In our study, we found that the 5-mm peri-tumor area contained many morphological changes in GC patients. These features included suspicious small lymph nodes and extramural venous invasion. Our findings suggested that a 5-mm peri-tumor area might provide many meaningful radiomics features. Due to the difficulty in distinguishing tumor tissues from the surrounding normal tissues, especially in patients with cachexia, we considered that a 5-mm area around the tumor might be relatively suitable. We found that the infiltration depth of the tumor was a heterogeneous biological characteristic, which increased with the progression of the disease. When tumor cells migrate outside the serosal layer, the possibility of LNM increases due to the rich lymphovascular network around the stomach [20].

The results of the multivariate analysis in the training/validation cohort revealed that the RS (C1+C2) value based on the tumor region and the 5-mm peri-tumor region model was the only independent risk factor for LNM, indicating a strong correlation between the radiomics features and the LNM status. However, the RS (C1+C2) value was not significant in the testing cohort (P = 0.064). This might be due to the lack of stability of our model, as the sample size used to construct and analyse the model was insufficient. Moreover, since the VOIs were sketched on CT images with 5-mm slice thickness, the thick-layer images might have added defects or distortions to some information, which affected the stability of the radiomics model.

The risk stratification based on the RS provided valuable information. The differences in the 5-year overall survival and progression-free survival between the high-risk and low-risk groups were statistically significant. In the training/validation cohort, the patients with low risk had ~2.2 times greater cumulative probability of survival than those with high risk. In the testing cohort, the cumulative progression-free survival probability in the low-risk group was 1.45 times higher than that in the high-risk group. Higher RSs were associated with poorer prognoses. Patients with high RSs had worse long-term survival and a higher tendency for early recurrence or progression, although they had received radical resection. Pathological tumor, node and metastasis (TNM) staging system is still the most reliable method to evaluate the long-term survival of GC patients [21], but such data can only be obtained after surgery. Improving the precision and individualization of treatment methods for GC is beneficial, especially for preoperatively screening patients with potential poor prognoses. Currently, the effectiveness of neoadjuvant therapy is still controversial,

especially for patients with locally advanced GC [22]. Neoadjuvant therapy is more suitable for high-risk subgroups [23]. Preoperative risk stratification based on the RS might help to identify patients who tend to have poor survival outcomes. Based on this information, neoadjuvant therapy might be administered before surgery, which might enhance the long-term survival of these patients.

There are still some limitations to the study. First, a patient was classified into the LNM-positive group if one lymph node was found to be metastatic through pathological examinations. However, the severity of LNM is also related to the number of lymph nodes involved. The eighth AJCC TNM staging system classified different N stages based on the number of metastatic lymph nodes [9]. Patients with different N stages might benefit from undergoing different extents of lymphadenectomy or neoadjuvant treatment [24]. We aim to investigate the relationship between the peri-tumor radiomics features and the number of metastatic lymph nodes in the future, since the peri-gastric area contains a portion of the lymphatic drainage system, and the radiomics approach might provide important information. Second, we only used data from a single institute. A large number of participants is required to build a reliable predictive model; as the number of cases enrolled in the internal training/validation cohort in this study was insufficient, our radiomics model had some instabilities. The results from the independent testing cohort showed the trend we expected; however, the overall outcomes were not satisfactory. In the future, large-scale multicenter studies are needed to further validate the effectiveness of radiomics models. Third, the CT images for investigation were acquired from different machines in our institute, and the scanning parameters of these machines were slightly different, which resulted in some confounding factors. Fourth, the region of interest was delineated from 5-mm slice-thickness images. The radiomics features extracted from these images have some deviations, which ultimately affected the performance of the prediction model.

Conclusions

To summarize, the radiomics model based on the combination of the tumor region and the 5-mm peri-tumor region showed good predictive efficiency for LNM. This method was better than the traditional CT evaluation method and the radiomics model containing features only from tumor tissue. The RS was strongly correlated with 5-year overall survival and progression-free survival of GC patients. Our study provided a comprehensive radiomics model for identifying metastatic lymph nodes and estimating survival outcomes. Our findings might have potential clinical value for evaluating the severity and prognosis of GC using a non-invasive method.

Authors' Contributions

Y.Y. made substantial contributions to the drafting of this manuscript and was responsible for the statistical analysis of this study. H.C. worked with J.W. on the collection of patients' information and the conduct of follow-up observation. M.J. made great efforts in the construction of models and offered instructions on the interpretation of data. X.C. collated the data of this study and selected appropriate cases for presentation. F.L. and S.R. contributed to the conception of this study and the revision of the manuscript.

Conflict of Interest

All authors have read and approved the submission to this journal and declared no competing interests. We declare that we have no financial and personal relationships with other people or organizations that can inappropriately influence our work.

References

1. Fitzmaurice C, Dicker D, Pain A *et al.*; Global Burden of Disease Cancer Collaboration. The global burden of cancer 2013. *JAMA Oncol* 2015;**1**:505–27.
2. Ajani JA, D'Amico TA, Almhanna K *et al.* Gastric cancer, version 3.2016, NCCN clinical practice guidelines in oncology. *J Natl Compr Canc Netw* 2016;**14**:1286–312.
3. Wang FH, Shen L, Li J *et al.* The Chinese Society of Clinical Oncology (CSCO): clinical guidelines for the diagnosis and treatment of gastric cancer. *Cancer Commun (Lond)* 2019; **39**:10.
4. Kim AY, Kim HJ, Ha HK. Gastric cancer by multidetector row CT: preoperative staging. *Abdom Imaging* 2005;**30**:465–72.
5. Kim HJ, Kim AY, Oh ST *et al.* Gastric cancer staging at multi-detector row CT gastrography: comparison of transverse and volumetric CT scanning. *Radiology* 2005;**236**:879–85.
6. Feng QX, Liu C, Qi L *et al.* An intelligent clinical decision support system for preoperative prediction of lymph node metastasis in gastric cancer. *J Am Coll Radiol* 2019;**16**:952–60.
7. Dong D, Fang MJ, Tang L *et al.* Deep learning radiomic nomogram can predict the number of lymph node metastasis in locally advanced gastric cancer: an international multicenter study. *Ann Oncol* 2020;**31**:912–20.
8. Tan CH, Vikram R, Boonsirikamchai P *et al.* Extramural venous invasion by gastrointestinal malignancies: CT appearances. *Abdom Imaging* 2011;**36**:491–502.
9. Amin MB, Greene FL, Edge SB *et al.* The Eighth Edition AJCC Cancer Staging Manual: continuing to build a bridge from a population-based to a more "personalized" approach to cancer staging. *CA Cancer J Clin* 2017;**67**:93–9.
10. Sun R, Limkin EJ, Vakalopoulou M *et al.* A radiomics approach to assess tumour-infiltrating CD8 cells and response to anti-PD-1 or anti-PD-L1 immunotherapy: an imaging biomarker, retrospective multicohort study. *Lancet Oncol* 2018; **19**:1180–91.
11. Wang Y, Liu W, Yu Y *et al.* CT radiomics nomogram for the preoperative prediction of lymph node metastasis in gastric cancer. *Eur Radiol* 2020;**30**:976–86.
12. Borggreve AS, Goense L, Brenkman H *et al.* Imaging strategies in the management of gastric cancer: current role and future potential of MRI. *Br J Radiol* 2019;**92**:20181044.
13. Thoeny HC, Froehlich JM, Triantafyllou M *et al.* Metastases in normal-sized pelvic lymph nodes: detection with diffusion-weighted MR imaging. *Radiology* 2014;**273**:125–35.

14. Ruys AT, Kate FJ, Busch OR *et al*. Metastatic lymph nodes in hilar cholangiocarcinoma: does size matter? *HPB (Oxford)* 2011;**13**:881–6.

15. Zhang Z, Zheng B, Chen W *et al*. Accuracy of (18)F-FDG PET/CT and CECT for primary staging and diagnosis of recurrent gastric cancer: a meta-analysis. *Exp Ther Med* 2021;**21**:164.

16. Bedard PL, Hansen AR, Ratain MJ *et al*. Tumour heterogeneity in the clinic. *Nature* 2013;**501**:355–64.

17. Sala E, Mema E, Himoto Y *et al*. Unravelling tumour heterogeneity using next-generation imaging: radiomics, radiogenomics, and habitat imaging. *Clin Radiol* 2017;**72**: 3–10.

18. Zwanenburg A, Vallières M, Abdalah MA, Aerts H *et al*. The image biomarker standardization initiative: standardized quantitative radiomics for high-throughput image-based phenotyping. *Radiology* 2020;**295**:328–38.

19. Beig N, Khorrami M, Alilou M *et al*. Perinodular and intranodular radiomic features on lung CT images distinguish adenocarcinomas from granulomas. *Radiology* 2019;**290**:783–92.

20. Zhang CD, Ning FL, Zeng XT *et al*. Lymphovascular invasion as a predictor for lymph node metastasis and a prognostic factor in gastric cancer patients under 70 years of age: a retrospective analysis. *Int J Surg* 2018;**53**:214–20.

21. Ji X, Bu ZD, Yan Y *et al*. The 8th edition of the American Joint Committee on Cancer tumor-node-metastasis staging system for gastric cancer is superior to the 7th edition: results from a Chinese mono-institutional study of 1663 patients. *Gastric Cancer* 2018;**21**:643–52.

22. Shin J, Lim JS, Huh YM *et al*. A radiomics-based model for predicting prognosis of locally advanced gastric cancer in the preoperative setting. *Sci Rep* 2021;**11**:1879.

23. Coccolini F, Nardi M, Montori G *et al*. Neoadjuvant chemotherapy in advanced gastric and esophago-gastric cancer: meta-analysis of randomized trials. *Int J Surg* 2018;**51**:120–7.

24. NCCN Guidelines Gastric Cancer, *NCCN clinical practice guidelines in oncology – Gastric Cancer*. National Comprehensive Cancer Network (NCCN) Guidelines. http://www.nccn.org/ (16 December 2022, date last accessed).